Electrochimica Acta 464 (2023) 142847

Contents lists available at ScienceDirect

Electrochimica Acta

journal homepage: www.journals.elsevier.com/electrochimica-acta

In-situ imaging and electrochemical monitoring of damaged thermal spray aluminium coating in synthetic seawater

Adriana Castro-Vargas [a,b,c,*], Shiladitya Paul [a,d,*]

[a] *Materials Innovation Centre, School of Engineering, University of Leicester, University Road, Leicester LE1 7RH, United Kingdom*
[b] *NSIRC, TWI Ltd, Granta Park, Great Abington, Cambridge CB21 6AL, United Kingdom*
[c] *Facultad de Ingeniería, Universidad Tecnológica de Bolívar, Km 1 Vía Turbaco, Cartagena 130011, Bolívar, Colombia*
[d] *Materials Performance & Integrity Group, TWI Ltd., Granta Park, Cambridge CB21 6AL, United Kingdom*

ARTICLE INFO

Keywords:
Thermal spray aluminium
Synthetic seawater
In-situ optical analysis

ABSTRACT

This paper presents the results of a study that combined electrochemical monitoring with *in-situ* imaging of Thermal Spray Aluminium (TSA) coating in synthetic seawater at room temperature in quiescent condition. The coatings were obtained by twin-wire arc spraying of 1050 aluminium alloy on S355 carbon steel substrate. TSA-coated steel samples were evaluated by analysing sequential images of the surface: (i) without defect; (ii) with defects machined before immersion (5% and 30% of exposed steel surface); (iii) with a defect machined after 35 d of immersion (10% of exposed steel surface); and (iv) after the removal of calcareous deposits formed on top of the exposed steel surface. Variations in the coating and the defect were captured and correlated with the evolution of Open Circuit Potential (OCP) during 35 days of full immersion. Determination of calcareous deposit formation time on the top of exposed steel was also carried out. The defect created before immersion impacted the cathodic reactions, resulting in a faster formation of corrosion products and calcareous deposits compared to the defect machined after exposure to synthetic seawater. The penetration time of the electrolyte in the coating and the activation of the surface are key in the protection mechanism and the kinetics of corrosion.

1. Introduction

A widely used coating system that offers cathodic protection to immersed steel structures in marine environments is thermally sprayed aluminium (TSA) [1–3]. TSA coatings, also known as sacrificial coatings, are galvanically more active than steel; therefore, they can protect steel even when damaged. The ability of TSA to polarise exposed steel to protective potentials, (according to DNV-RP-B401 [4], without excessive consumption of the coating has been adopted to define the damage tolerance of such coatings [5].

Till date, the damage tolerance research of TSA coating, has focused on evaluating small defects (typically exposing steel, ~1-5% of the specimen area), machined before the exposure to the simulated marine environment [6–8]. The defect size in the specimens replicates the most likely area ratio of damage that can occur during the installation, handling, or transport of offshore structures [6]. However, most studies have only analysed intentional defects machined before immersion, but no work reports results when defects are machined post-exposure.

Laboratory and offshore testing of TSA (AA1050) with 5% of surface area defect were reported by Grinon et al. [7]. The evolution of Open circuit Potential (OCP) was recorded for over 50 days. In both conditions, TSA provided cathodic protection. In another study [9], a steel sample was coated with TSA in only 10% of the area exposed to synthetic seawater, the potential was recorded for 100 days at room temperature. The notable finding was the ability of TSA to protect the exposed steel (90%) within the first 35 days. However, the quantification of the damage level that TSA can tolerate is not fully explored. It is important to understand the protection mechanism provided by the TSA in an extreme damage scenario due to the polarization of steel may be insufficient to protect it, or the consumption of TSA can be higher due to the anodic nature of the coating [9].

In laboratory studies [6-8,10], TSA-coated steel coupons with damage, were inspected after exposure to synthetic seawater; typically, it has been found after testing, that the defect zone was covered by white deposits without signs of rust or corrosion, while the top of the coated surface was covered by aluminium corrosion products and calcareous deposits. The characterisation of the cross-section and corrosion products/deposits were conducted by Scanning Electron Microscopy (SEM),

* Corresponding authors.
E-mail addresses: acv6@leicester.ac.uk (A. Castro-Vargas), shiladitya.paul@twi.co.uk (S. Paul).

https://doi.org/10.1016/j.electacta.2023.142847
Received 29 December 2022; Received in revised form 14 May 2023; Accepted 6 July 2023
Available online 14 July 2023

Energy Dispersive X-ray spectroscopy (EDX), and X-ray Diffraction (XRD). This approach is helpful for obtaining information on the final degradation post-exposure; however, it does not provide real-time information about the corrosion process.

Based on those findings, the mechanism of protection of steel by damaged TSA can be summarized as follows [11]: TSA provides cathodic protection by galvanic action; (TSA as anode and exposed steel as cathode), causing the dissolution of Al (Equation 1).

$$Al \rightarrow Al^{3+} + 3e^- \quad (1)$$

On the cathodic surface, the oxygen reduction and/or hydrogen evolution take place Equation 2 and (3);

$$O_2 + 2H_2O + 4e^- \rightarrow 4OH^- \quad (2)$$

$$2H_2O + 2e^- \rightarrow H_2 + 2OH^- \quad (3)$$

Consequently, the local pH increases due to the production of OH^- ions promoting the co-precipitation of insoluble compounds rich in magnesium and calcium on the exposed steel described by the reactions in Equation 4,5, and 6. It is well known that the calcareous deposits formed at room temperature on cathodically protected steel comprise an inner layer of brucite ($Mg(OH)_2$) and an outer layer of aragonite ($CaCO_3$) [6], and the mechanism is somewhat known under certain conditions [12–14]. The potentials that favour the formation of said calcareous deposits are reported as follows: (i) Aragonite precipitates at potentials between -0.9 V and -1.1 V (SCE), (ii) Brucite (first layer) and Aragonite (second layer) are formed at -1.2 V (SCE) and (iii) Brucite is formed at potentials more negative than -1.3 V (SCE) [15]. The temperature and constituents of seawater determine the nature of the deposits. Depending on the morphology and pore architecture, such deposits could provide barrier properties that prevent diffusion of dissolved oxygen, adding protection to exposed steel [8,16].

$$OH^- + HCO_3^- \rightarrow H_2O + CO_3^{2-} \quad (4)$$

$$CO_3^{2-} + Ca^{2+} \rightarrow CaCO_3 \quad (5)$$

$$Mg^{2+} + 2OH^- \rightarrow Mg(OH)_2 \quad (6)$$

Aluminium corrosion products and calcareous deposits precipitate on the surface as well as inside the pores of the coating, providing the plugging effect, which reduces the self-corrosion of aluminium [17,18]. Over time, white corrosion products of Al oxides and hydroxides appear on the surface of TSA. The overall Al dissolution reaction is given in Equation 7, which is a combination of the reactions given in Equations 1, 8, and 9. For simplicity, precipitation of $Al(OH)_3$ has been assumed; however, compounds such as AlOOH and Al_2O3 are also possible [19].

$$Al + 4H_2O + e^- \rightarrow Al(OH)_4^- + 2H_2 \quad (7)$$

$$Al + 3OH^- \rightarrow Al(OH)_3 + 3e^- \quad (8)$$

$$Al(OH)_3 + OH^- \rightarrow Al(OH)_4^- \quad (9)$$

The long-term performance of TSA coatings depends on the stability and formation time of the calcareous deposits. It must be considered that the porosity and resistivity of the said protective layer change over time. The deposits also can be removed by the ocean currents or by common maintenance operations. For example, inspecting offshore structures requires prior cleaning to remove marine growth, generally, a high-pressure water jet system is used [20]; also, during inspection mooring of boats might cause damage.

The nature of TSA coatings is complex, due to the porosity, anodic trend, roughness, etc. As described above, the protection mechanism offered by the TSA coating with exposed steel surface in artificial seawater involves multiple and simultaneous reactions, which makes it a difficult subject to study, increasing the risk of misinterpretation of electrochemical data in corrosion research. Nonetheless, the common electrochemical testing techniques, such as monitoring of the Open Circuit Potential (OCP), Linear Polarisation Resistance (LPR) and Electrochemical Impedance Spectroscopy (EIS), have been used to assess the behaviour of TSA [21–24]. Some authors acknowledge the difficulty in distinguishing cathodic and anodic reactions and warn about the limitations of said techniques in obtaining quantitative data on damaged TSA corrosion rate [6,11].

To address the above knowledge gap, a systematic study involving simultaneous *in-situ* imaging and OCP monitoring was carried out to obtain insight into the protection mechanism provided by TSA in the presence of defects, inspecting the surface activity and macroscopic related phenomena in parallel with the evolution of the potential. The study allowed the introduction of comparative plots, correlating the OCP with the corrosion process in damaged TSA. These results might help to improve the interpretation of the measured electrical signals during immersion in further studies using more advanced electrochemical techniques.

2. Experimental

2.1. Sample Preparation and Materials

BS EN S355J2 Carbon - Manganese steel coupons of 75 mm x 75 mm x 6 mm were cut, and the surface was prepared by grit blasting with angular alumina (NK36 type and 100 psi air pressure) to achieve standard cleanliness of Sa 3, according to ISO8501-1 [25]. The 300 μm thick coating was obtained by Twin Wire Arc Spray (TWAS) process with an ARC140 gun (Metallisation Ltd., Dudley, UK) following the parameters shown in Table 1. In the process, two wires of (AA1050 alloy, 99.5 wt% Al), are forced to establish an electrical arc. The molten or semi-molten material is then accelerated and sprayed onto the substrate by an atomising gas stream. Table 2 shows the nominal composition of the substrate and coating in weight %. The roughness of the substrates and the TSA coating was measured three times using a 3D profilometer (Alicona InfiniteFocusSL). The average roughness (Ra) of the substrate was 13 ± 5 μm, while the coatings recorded 40 ± 5 μm.

2.1.1. Cases of study

Fig. 1 schematically shows the identification of the samples evaluated in this work. Intentional defects (0.8 mm deep blind holes), also referred to as exposed steel, were machined with a flat slot drill in the center of TSA-coated steel samples. The electrical connection was made by inserting threaded rods (4 mm diameter) on one side of the sample. Note that the exposed surface area to the synthetic seawater is only 10 cm^2; therefore, the defect diameters vary in each case, as described below:

- A0: TSA without exposed steel.
- A-10: TSA with 10% of exposed steel. After 35 days of exposure, sample A0 was rinsed with deionized water, and an 11 mm diameter defect was machined. The sample A-10 was placed in the cell (see Fig. 2) and fresh synthetic seawater was introduced for the optical-electrochemical monitoring test.
- B5: TSA with 5% of exposed steel. An 8 mm diameter defect was machined before the exposure to synthetic seawater.
- C30: TSA with 30% of exposed steel. A 19 mm diameter defect was machined before the exposure to synthetic seawater.
- C-30R: TSA with 30% of exposed steel and reactivation of the cathodic surface by removing the calcareous deposits formed on top of the steel in sample C30 after 35 d of exposure. The sample was rinsed with deionized water, and calcareous deposits were removed using a commercial rotary tool. First, the surface was carefully cleaned with a plastic brush, avoiding the edges of the coating. Subsequently, a disc of wool felt was used to remove the calcareous matter. The sample C-30R was placed in the cell (see Fig. 2), and the

Table 1
Thermal spray process parameters.

Wire diameter (mm)	Wire feed rate (m/min)	Spray distance (mm)	Increment step (mm)	Horizontal speed (mm/s)	Voltage (V)	Current (A)
2.3	5	125	10	450	30	220

Table 2
Nominal composition of the substrate and coating in wt. %.

Material	Element wt.%									
	C	Mn	S	Si	P	Al	Cu	Zn	Mg	Fe
Substrate S355	0.12	1.39	0.019	0.39	0.014	0.035	0.170	-	-	Balance
Coating AA 1050	-	-	-	0.07	-	99.5	0.02	0.05	0.05	0.21

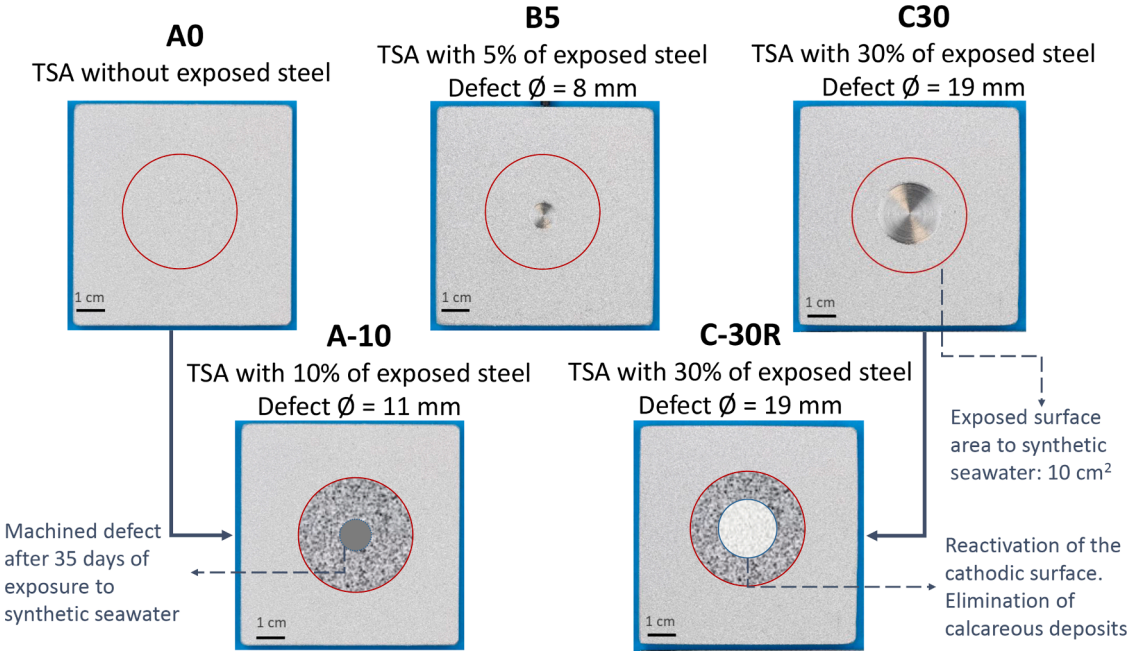

Fig. 1. Samples identification.

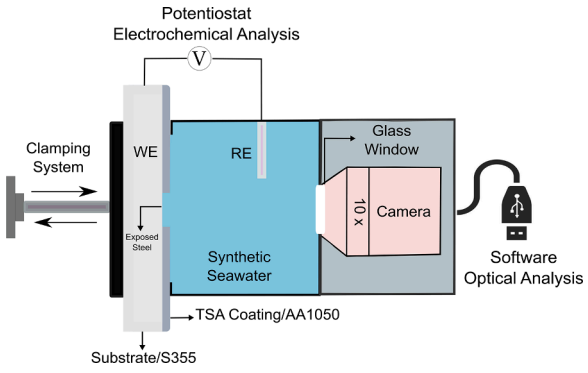

Fig. 2. Illustration of the Optical - Electrochemical cell.

optical-electrochemical monitoring test was performed with fresh synthetic seawater.

2.2. *In-situ Imaging and Electrochemical Monitoring*

2.2.1. *Optical Inspection*

The tests were carried out using an Optical-Electrochemical Cell (Correlimage® Corrosion Imager V1.0 and image recognition software. Delft, Netherlands). Fig. 2 illustrates the cell setup. On the left, the coated sample is placed vertically, and the system allows clamping it to the cell. A 36 mm O-ring diameter was used to prevent leakage. On the right side, a transparent Plexiglas window aligns the studied sample with the camera, thereby optically inspecting the samples in real-time while they are exposed to synthetic seawater. The optical system includes a LED light placed parallel to the glass window to illuminate the exposed area (10 cm^2). The tank can be filled with 250 ml of electrolyte; holes hold the reference electrode and the pH meter in the upper part.

The integrated camera with 15 microns per pixel resolution and settings of brightness 0, contrast 1, hue 0 and saturation 18 was used to capture images every 2 hours from the start of the immersion. The surface activity was processed and analysed in all cases using a jet colour map and a contrast multiplier of 1.715. The images were exported at the highest resolution and the colour scale (from royal blue to red) indicates the level of surface activity.

2.2.2. OCP Monitoring

The Open Circuit Potential (OCP) was recorded every 10 min during 35 d of exposure under stagnant conditions, and at room temperature (18 ± 2°C) using a VSP 300 BioLogic potentiostat and EC-Lab software. TSA-coated steel samples were used as working electrodes; synthetic seawater following ASTM D1141-98 (pH 7.8 ± 0.3, conductivity 4.8 S/m) as the electrolyte, whose composition can be seen in Table 3; and Ag/AgCl (Sat. KCl) as the reference electrode. The pH of the solution was measured weekly during the tests; the variations were minimal over time, with values between 7.68 and 7.92. Finally, hundreds of pictures were collected and thoroughly inspected in each case. However, in this article only the most representative images were selected and correlated with changes in OCP. Additional processed images and videos can be found in the link provided in the supplementary materials section.

3. Results

To facilitate the understanding of the results, it is important to note that:

- Potentials in this paper are referred to against Ag/AgCl (sat. KCl) reference electrode ($E_{ref} = +0.199$ V vs SHE) unless otherwise stated.
- The recommended practice DNV-RP-B401 [4], advises that -0.8 V Ag/AgCl (seawater) equivalent to -0.743 V Ag/AgCl (sat. KCl), is accepted as the design protection potential for carbon and low-alloy steels; therefore, -0.743 V will be referred to as the protective potential.

3.1. TSA without damage (A0)

Fig. 3 integrates the results from the *in-situ* inspection and electrochemical monitoring showing the evolution of OCP and the images obtained over time. At the beginning of the immersion, the potential was -0.812 V, followed by a drastic drop towards more negative values in a few hours. At this stage, the degradation of the air-formed oxide layer of TSA begins, increasing the aluminium dissolution rate (Equation 1). After 10 h, a potential of -1.014 V was recorded. It can be observed in the sequential images of Fig. 3b that the coating keeps a metallic shine appearance, and the gradual activation of aluminium is identified by localised colour changes in the processed image.

After 1 d of testing, the potential evolves to -1.048 V, the aluminium activity increases, and a constant and uniform bubbling begins on the surface. The literature reports that the corrosion potential of TSA in seawater is approximately -1.2 V [6,17]; however, this value is reached after the first day of immersion and substantial surface activation. In this case, a potential of -1.168 V was recorded after 3 d. At this point, a matt grey colour predominates, with some small areas maintaining a bright grey colour due to the high porosity and roughness of the TSA.

From 5 d onwards, the potential increases progressively, and the level of bubbling decreases, as can be observed in the captured image after 15 d of testing and potential of -1.034 V. A matte grey colour and high surface activity in the original and processed image, respectively, combined with the trend towards less negative potentials values, suggest the formation of a protective layer of aluminium corrosion products and/or calcareous deposits on the surface as well as inside the pores reducing the self-corrosion of Al. The sample remains very stable from 18 d with minimal variations in potential and imperceptible surface activity, as shown in Fig. 3c. This status lasts up to 35 d of the trial. Clearly, in this period the curve reaches a plateau around -0.997 V. See Fig. 3a.

Table 3
Synthetic seawater composition according to ASTM D1141-98 [26].

Compound	Salt Concentration (g/L)	Compound	Salt Concentration (g/L)
NaCl	24.53	$NaHCO_3$	0.201
$MgCl_2$	5.2	KBr	0.101
Na_2SO_4	4.09	H_3BO_3	0.027
$CaCl_2$	1.16	$SrCl_2$	0.025
KCl	0.695	NaF	0.003

3.2. TSA with 10% of exposed steel (A-10)

It can be seen in Fig. 4a the potential was -0.797 V at the beginning of the immersion; however, it decreased rapidly, and after 3 h the potential reached a value of -0.902 V. Small bubbles appeared only in the region adjacent to the defect and the surface activity increased slightly, being more evident around the exposed steel as can observe in Fig. 4b, 3 h. The tool used to create the defect most likely reactivated the surface surrounding the exposed steel.

After 2 d of testing, the potential dropped to -0.969 V, and only a few bubbles appeared in the coated region, despite the pores were clogged with aluminium corrosion products, the increase of the pH can lead to the dissolution of the air-formed oxide, exposing the new aluminium surface to seawater enable the generation of hydrogen [19]. The beginning of the precipitation of calcareous deposits on the top of the defect was also optically recognisable.

After 4 d, the exposed steel area is covered with deposits; the bubbling and the evolution of the potential towards a more negative value (-1.002 V), indicate hydrogen generation in the cathodic zone. The software detected small changes on the coated part, which provides evidence that the active aluminium protects the exposed steel.

A potential of -0.980 V was recorded after 7 d. From this moment, the surface activity is almost constant with no bubbles in the defect or coating. The colour contrast allows the recognition of a denser layer of deposits that are preferentially located at the bottom of the tank due to the effect of gravity.

The OCP then stabilised with minimal fluctuations from 8 d to 30 d, with values between -0.958 V and -0.965 V, correspondingly. In the further optical analysis conducted during this period (Fig. 4c), the software did not detect significant changes: nevertheless, observing the processed image thoroughly, tiny points remain active in the coated region, while the defect region is entirely inactive, confirming that the deposits act as a physical barrier.

Fig. 5, compares the evolution of the OCP of TSA before and after machining the defect. The potential of TSA with exposed steel reached a plateau faster than the TSA sample without defects. In both cases, the potential stabilised around similar values, -0.997 V in A0 and -0.965 V in A-10. The activation of TSA when the defect is created post-exposure can be clearly related to the drop in potential in the first 4 d, demonstrating the ability of TSA to protect steel.

3.3. TSA with 5% of exposed steel (B5)

At the beginning of the test, the potential was -0.702 V and the system reached the recommended protective potential (-0.743 V), only after 2 h. Therefore, the exposed steel was above the protection potential for at least this period. During experimentation, light green colouration was observed in the defect and the solution in the vicinity of the defect (original image), which indicates an initial dissolution of iron (Equation 10).

$$Fe \rightarrow Fe^{+2} + 2e^{-} \quad (10)$$

After 6 h, the potential was -0.816 V, and the aluminium surface was activated progressively. The electrolyte penetration into the coating is not uniform since some regions retain a metallic shine. The processed image reveals the effect of gravity during the initial oxidation of the iron.

Bubbling in the exposed steel and coating was observed on day 1 of

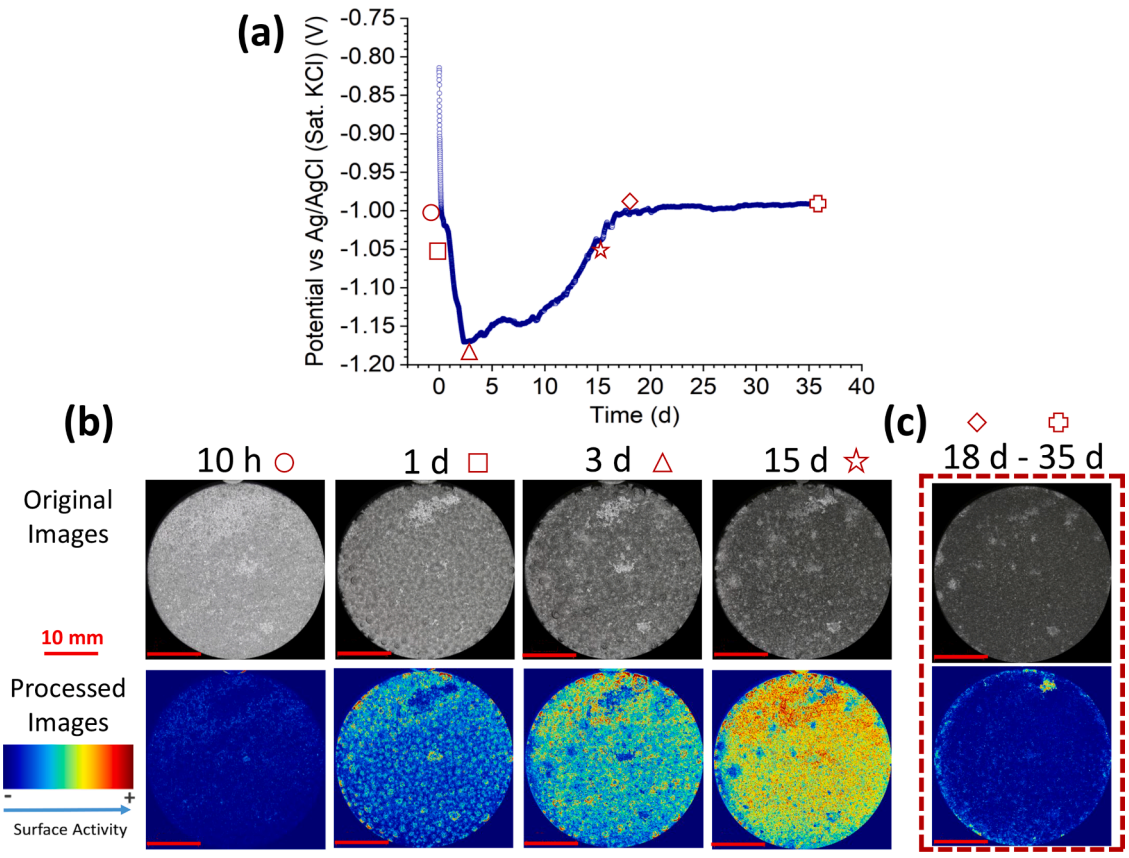

Fig. 3. Optical-Electrochemical monitoring of TSA without damage (A0). **(a)** Record of OCP. **(b)** Original and processed sequential images. **(c)** Optical analysis from 18 d to 35 d.

immersion and a potential of -1.011 V. Therefore, the active surface area of TSA could be masked and image recognition analysis should be performed with caution. Despite the intense bubbling, a notable increase in the activation of aluminium was identified. Rapid formation of calcareous deposits is observed after 2 d of testing and a potential of -1.068 V. At this potential, the cathodic reaction involves hydrogen evolution.

The potential rose slightly to -1.027 V after 13 d. The images obtained show fewer and smaller bubbles over the defect suggesting a decrease in the kinetics of the cathodic reactions. From the original image a dense matter of white deposits is identified over the defect, similarly a mixture of dark matt grey colour and bright grey colour is observed in the coated surface area. From 25 d to 35 d, the optical analysis showed no changes in the surface activity (see Fig. 6c) and the potential varied between -0.990 V and -0.971 V.

The performance of damaged TSA when the defect is machined before and after exposure differs substantially. When the defect is created after immersion (A-10 Fig. 4), the aluminium activates rapidly, the system reaches the range of protective potentials, and the precipitation of calcareous deposits takes 7 d. Conversely, when the defect is machined before the immersion (B5, Fig. 6), initial dissolution of iron occurs until the air-formed oxide layer degrades, the electrolyte penetrates the coating and, the aluminium surface is activated. The formation of calcareous deposits occurs within 2 d of exposure.

3.4. TSA with 30% of exposed steel (C30)

As mentioned before, during the initial exposure period, TSA is activated gradually by the degradation of the air-formed oxide layer. Therefore, the protection of steel by TSA is not immediate, so iron oxidation occurred within the first few hours and the protective potential was reached 7 h after the start of the test, as described in section 3.3.

The original image in Fig. 7b captured after 1 d of exposure shows a slight sign of iron corrosion products. After 1 d, the potential reached a value of -0.940 V, providing evidence of the high damage tolerance of TSA.

The potential increased from 2 d to 4 d with values of -1.019 V and -0.986 V, respectively. This trend is correlated with the formation of a fine layer of calcareous matter by inspecting the sequential images in Fig. 7b. The effect of gravity seems to play an important role when a large defect is studied. It can be noted in Fig. 7b, 4 d that the calcareous deposits are preferentially located in the lower region of the defect. At the same time, the upper part is left without the protective layer. After 14 d, the calcareous deposits layer is denser and the potential rose to -0.925 V.

During the potential stabilisation period (from 15 d to 33 d), the same behaviour of inactivity seen in the above cases was determined by further optical analysis, as shown in Fig. 7c. Finally, the potential after 33 d recorded a value of -0.938 V. In the C30 case, the intensity and amount of bubbling in the exposed steel are clearly less than in the B5 case. The precipitation time of a uniform layer of calcareous deposits on the defect was around 10 d, while in case B5 it took only 2 d.

3.5. TSA with 30% of exposed steel after removing the calcareous deposits (C-30R)

At the beginning of the immersion, no iron dissolution was evident. The drop of potential from -0.752 V to -0.821 V occurred in 2 h (see Fig. 8a) without significant changes as can be seen in the captured image, Fig. 8b.

After 1 d, the potential was -0.850 V, and the TSA was activated predominantly in the contiguous region of the defect. A fine layer of deposits was identified with the help of the software. No bubbling in the

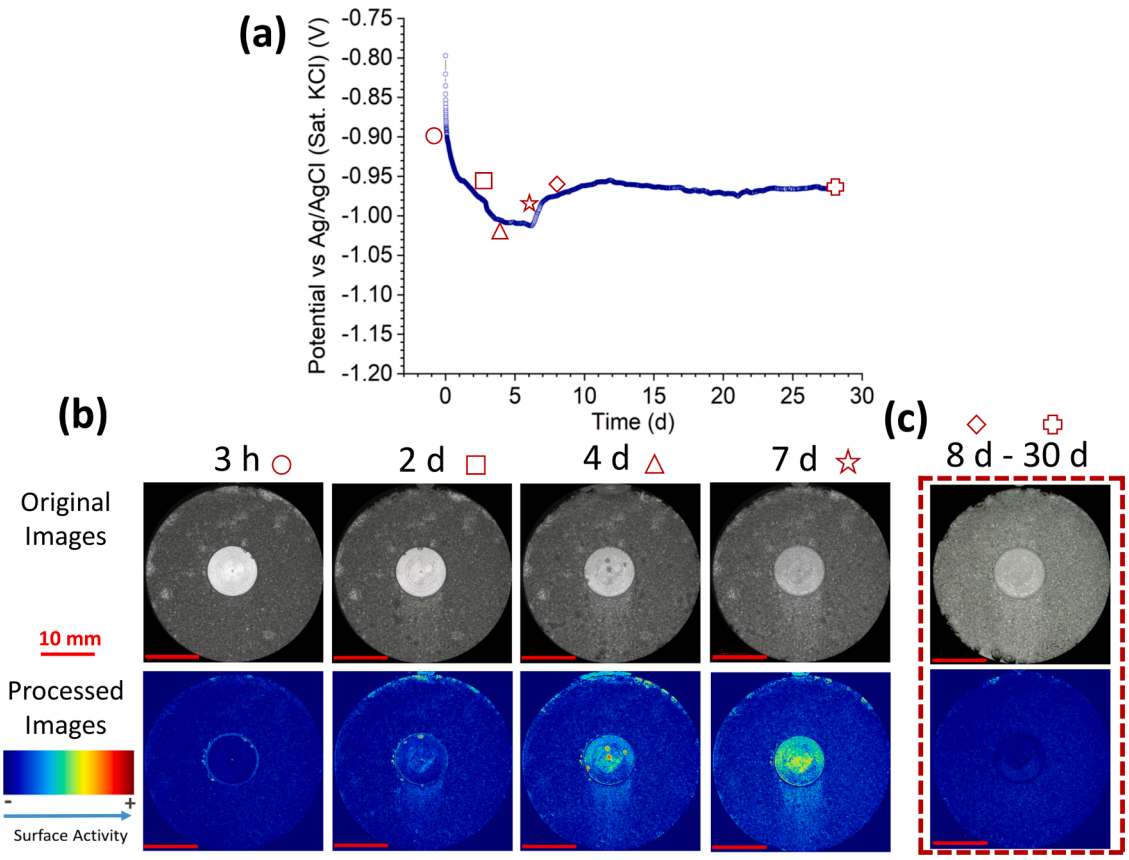

Fig. 4. Optical-Electrochemical monitoring of TSA with 10% of exposed steel (A-10). **(a)** Record of OCP. **(b)** Original and processed sequential images. **(c)** Optical analysis from 8 d to 30 d.

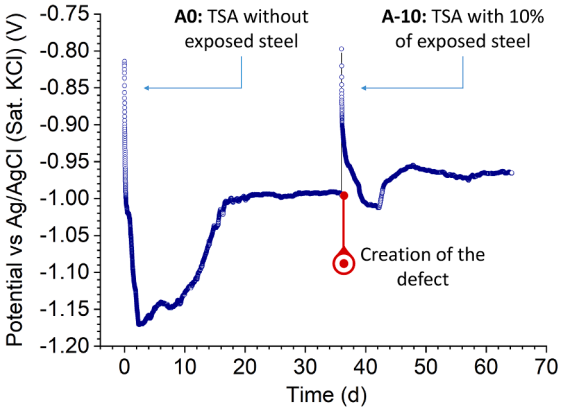

Fig. 5. OCP evolution before and after machining the defect. Samples A0 and A-10, respectively.

coating or defect was detected since at potentials less negative than -0.906 V, oxygen reduction is the predominant cathodic reaction and hydrogen evolution is thermodynamically less likely [12].

Due to the effect of gravity, the deposits formed first in the lower part of the defect, as can be seen in Fig. 8b (1 d and 8 d). After 8 d and a potential of -0.918 V, the layer of calcareous deposits grew and the surface activity in the coated part remained at very low levels. After 16 d and a potential of -0.916 V, the exposed steel zone is completely covered by a layer of calcareous matter. The optical analysis from 18 d (-0.918 V) to 30 d (-0.924 V) shown in Fig. 8c revealed a negligible activity, and stable potential reaching a value of -0.924 V after 30 d. The sample was covered by aluminium corrosion products and deposits without signs of rust, after 30 d of testing.

Fig. 9 compares the evolution of the OCP of damaged TSA (C30) followed by the removal of calcareous deposits formed on the exposed steel after exposure (C 30-R). Remarkably, the drop of potential is more pronounced in C30 than in C-30R; this trend could be attributed to the activation of TSA when the defect is machined before immersion. After the reactivation of the cathodic area, only a small portion of TSA is activated, and it is enough to polarise steel into the protective potentials range. In addition, the potential of stabilisation is very close in both cases, recording values of -0.938 V in C30 and -0.924 V in C-30R.

Table 4 compiles the formation time of calcareous deposits in the exposed steel, potential, and bubbling in the cases studied. The potentials recorded in each case demonstrated that TSA coatings protect offshore steel structures without external cathodic protection systems. The stabilisation of the potential obeys the mixed potential theory. The approximate value of the corrosion potential of TSA without exposed substrate in artificial seawater is -1.2 V, while the value for steel is -0.7 V [6,17], therefore the corrosion potential of TSA with exposed steel is between those values around - 0.97 V, as can be seen in Table 4. In the case of a large defect, the potential evolves to values further away from the TSA equilibrium potential (-0.924 V).

4. Discussion

4.1. Optical–electrochemical monitoring

TSA coatings are increasingly being used in offshore applications to mitigate corrosion. As the use of such coatings grows, the fundamental understanding of their behaviour becomes more critical. The use of optical devices to inspect corrosion processes as a complementary technique is not new; however, detailed macroscopic phenomena

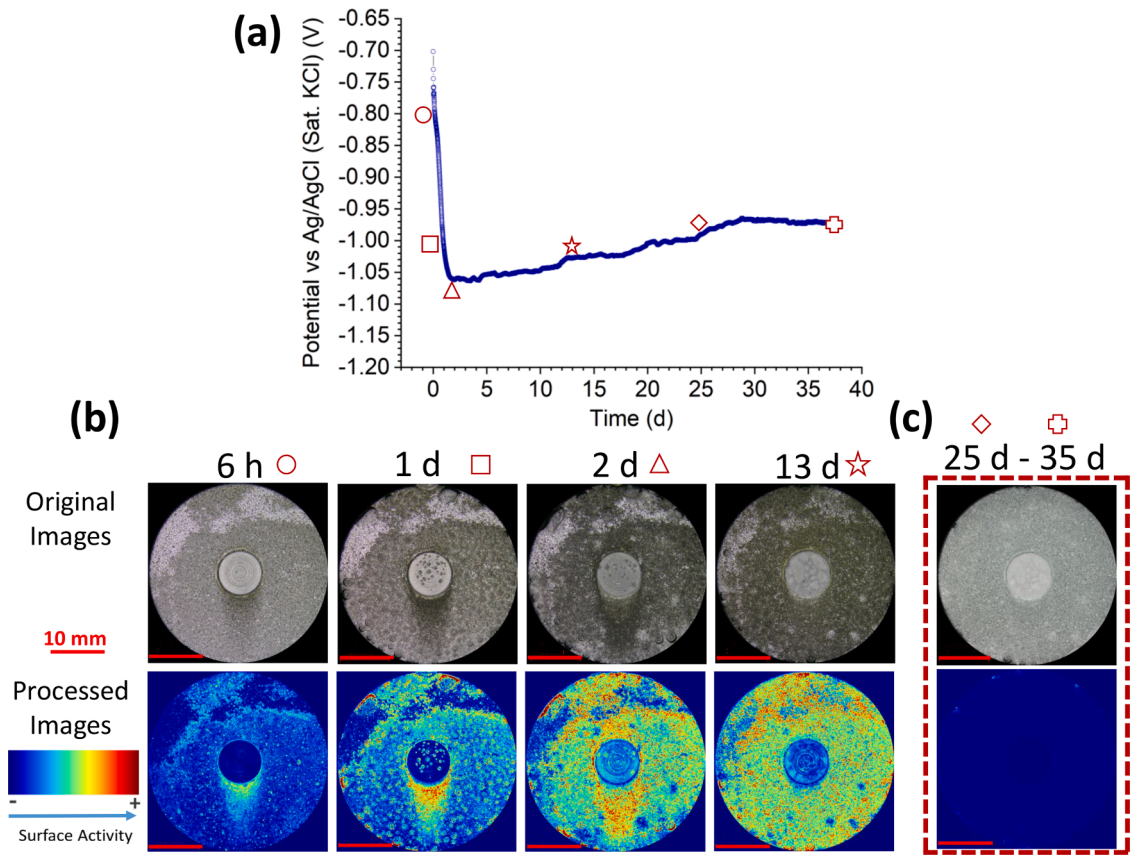

Fig. 6. Optical-Electrochemical monitoring of TSA with 5% of exposed steel (B5). **(a)** Record of OCP. **(b)** Original and processed sequential images. **(c)** Optical analysis from 25 d to 35 d.

related to damaged TSA coatings in real-time have not been reported in the open literature.

The results presented in this work revealed that some essential aspects, such as the high porosity and roughness of the TSA, lead to the non-homogeneous wettability of the studied surface. This characteristic was also observed in a study of TSA exposed to artificial seawater droplets to simulate splash zone conditions; this study also highlighted the need to evaluate TSA with pre-exposure to reach a stable potential [17]. Such features of TSA contribute to the gradual activation of aluminium as the air-formed layer degrades during the first few hours of immersion. This activation is associated with the drastic drop in the potential towards negative values in all cases evaluated in this work. The non-uniform aspect of the coating (metallic shine and matt appearance) during the initial stage was identified when the defect was machined before immersion.

This work also evaluated TSA when the defects were machined after exposure and when the calcareous deposits were removed. Such work has rarely been reported in the literature. In these cases, the protective potential was reached once the synthetic seawater was in contact with the specimen, indicating an excellent performance of TSA in case of damage during service.

The presence of bubbles in the coated area can be attributed to several reasons: (i) the penetration of the electrolyte into the coating and the displacement of trapped air from the pores; (ii) the dissolution of Al enables the generation of hydrogen Equation 7); and (iii) the generation of hydrogen gas if the synthetic seawater reaches the steel surface (cathode) through the interconnected pores of the coating. Previous studies have found aragonite on top of the coating after 30 d of exposure [6]. Therefore, this provides evidence that high porosity in the coating (10%-15%) [11,27,28] allows the contact between the substrate and electrolyte, promoting the cathodic reactions (Equations 2 and (3) on the substrate, and subsequently, the precipitation of calcareous deposits. The intensity of the bubbling in the defect area (exposed steel) could be associated with the kinetics of the cathodic reactions, being higher after Al activation and lower once the cathode surface is covered with calcareous deposits.

When the potential becomes more negative than -1.056 V, there is a greater possibility of hydrogen generation due to the dissociation of water (Equation 3), producing atomic hydrogen which can either combine, forming hydrogen gas or become absorbed into the metal [4, 14]. Cathodic protection of steel in offshore applications leads to hydrogen generation. This could be a cause for concern related to hydrogen embrittlement, especially with high-strength steel. Paul [19] studied the hydrogen localization on TSA-coated steel under cathodic protection. The hydrogen level in the TSA-coated steel was 100 times higher than that observed in the uncoated samples; therefore, the amount of hydrogen seems to be located mainly in the TSA layer or the TSA-steel interface [19]. However, it is unclear if this would negatively affect the performance of coated steels in service, and more research is needed.

The evolution of the potentials towards less negative values is directly associated with the precipitation of a layer of calcareous deposits on the exposed steel. The stabilisation of the potential and low surface activity recorded by the image recognition software corroborates the barrier properties of calcareous deposits, adding protection to the exposed steel. Furthermore, the potentials were in the range of protective potentials for steel, suggesting the high damage tolerance of TSA even in the presence of machined defects before and after immersion.

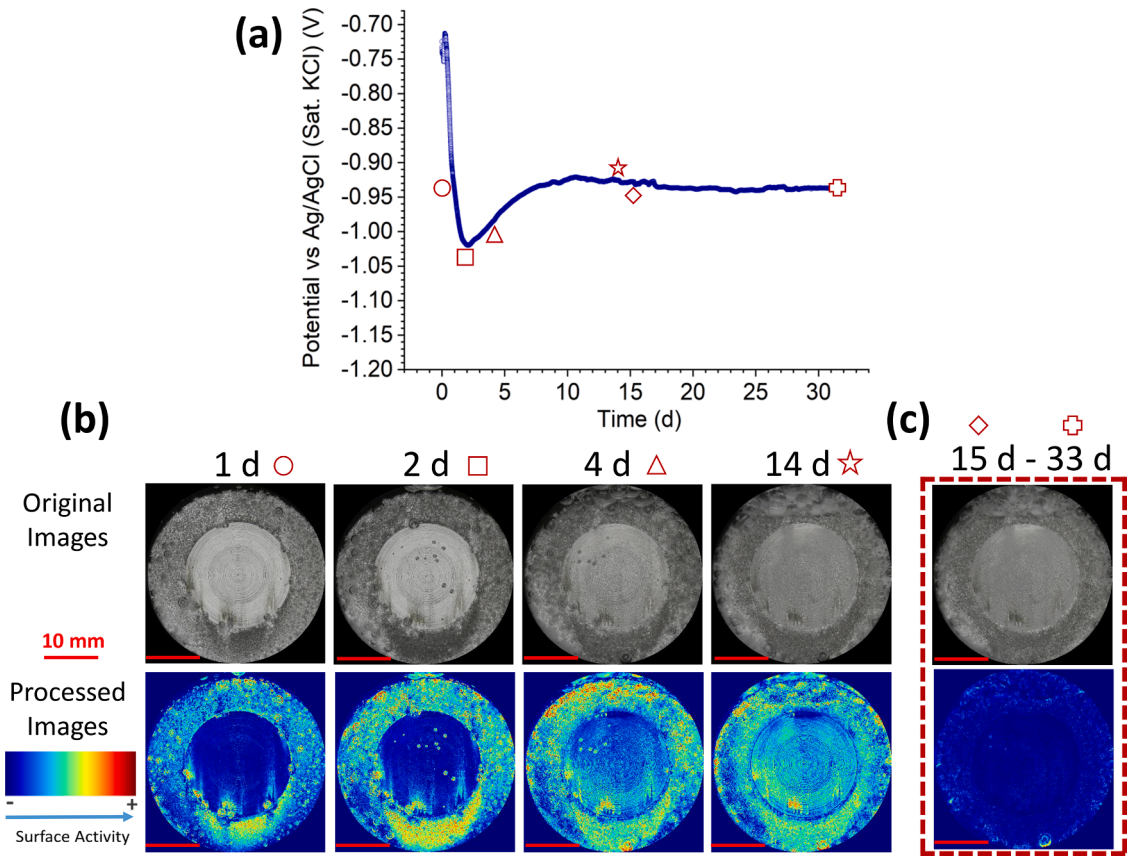

Fig. 7. Optical-Electrochemical monitoring of TSA with 30% of exposed steel (C30). **(a)** Record of OCP. **(b)** Original and processed sequential images. **(c)** Optical analysis from 15 d to 33 d.

4.2. Formation time of the calcareous deposits

It is known that the formation of calcareous deposits on steel contributes to the effectiveness of cathodic protection, acting as a barrier preventing oxygen reduction on the steel surface. Additionally, it has also been demonstrated that the hydrogen uptake is reduced when a brucite deposit is predominantly formed on steel during cathodic protection; nonetheless, the ingress of hydrogen could take place within the initial 100 h of immersion [14]. The time it takes for calcareous deposits to form is crucial as they reduce the exposed surface area, limit oxygen diffusion, and restrict the ingress of hydrogen into steel. The approach used in this study enabled us to determine both the formation time of the protective layer on the surface of the exposed steel and the corresponding recorded potential for each case, as presented in Table 4. The structure, stability, and pore architecture of such deposits are critical in determining the damage tolerance and long-term performance of TSA.

The nature of the calcareous deposits depends on the seawater constituents, temperature, seawater velocity, and cathodic protection potential [8,15]. Natural seawater contains various species, a mixture of salts, nutrients and sediments. The composition varies according to the location, temperature, season, and depth. Marine growth and the presence of microorganisms add further complexity to the corrosion processes in marine environments. Keeping this in mind, the results presented in this work does not provide data in natural seawater, but give an idea of the performance of damaged TSA under simulated conditions. In light of our research objectives, synthetic seawater was selected as it contains the main species present in natural seawater (see Table 3). The presence of Ca^{2+}, Mg^{2+}, and SO_4^{2-} ions directly affects the formation of deposits and corrosion products. Therefore, to simulate marine conditions in TSA assessment, the use of 3.5 wt. % NaCl must be avoided [11].

4.3. Limitations and future work

Image recognition software examines the digital images collected using time-lapse photography and quantifies the percentage of surface activity over time. However, when dealing with damaged TSA (in our case), caution should be exercised in interpreting and quantifying data due to surface changes that may indicate the activation of aluminum, bubbling, precipitation of calcareous deposits, and/or corrosion products. Image analysis combined with the open circuit potential (OCP) data allowed better understanding of the corrosion process in damaged TSA in a simulated marine environment and quiescent conditions at room temperature. However, the corrosion rate, stability, formation time, and detachment of calcareous deposits may be affected by seawater flow. Additional research is required to address this knowledge gap and enhance our understanding of the performance of damaged TSA under flow conditions.

5. Conclusion

In-situ optical monitoring as a complementary technique allowed a better understanding of the mechanism of protection offered by TSA in presence of damage and its relation to the changes in potential during exposure to a simulated marine environment. The following conclusions can be drawn from the work presented in this paper:

- The high porosity and roughness of TSA coatings result in non-uniform wettability of the surface, which delays the stabilisation of the corrosion potential, especially in the absence of intentionally exposed steel. The TSA sample with exposed steel reached a plateau in potential faster than the TSA sample without defect.

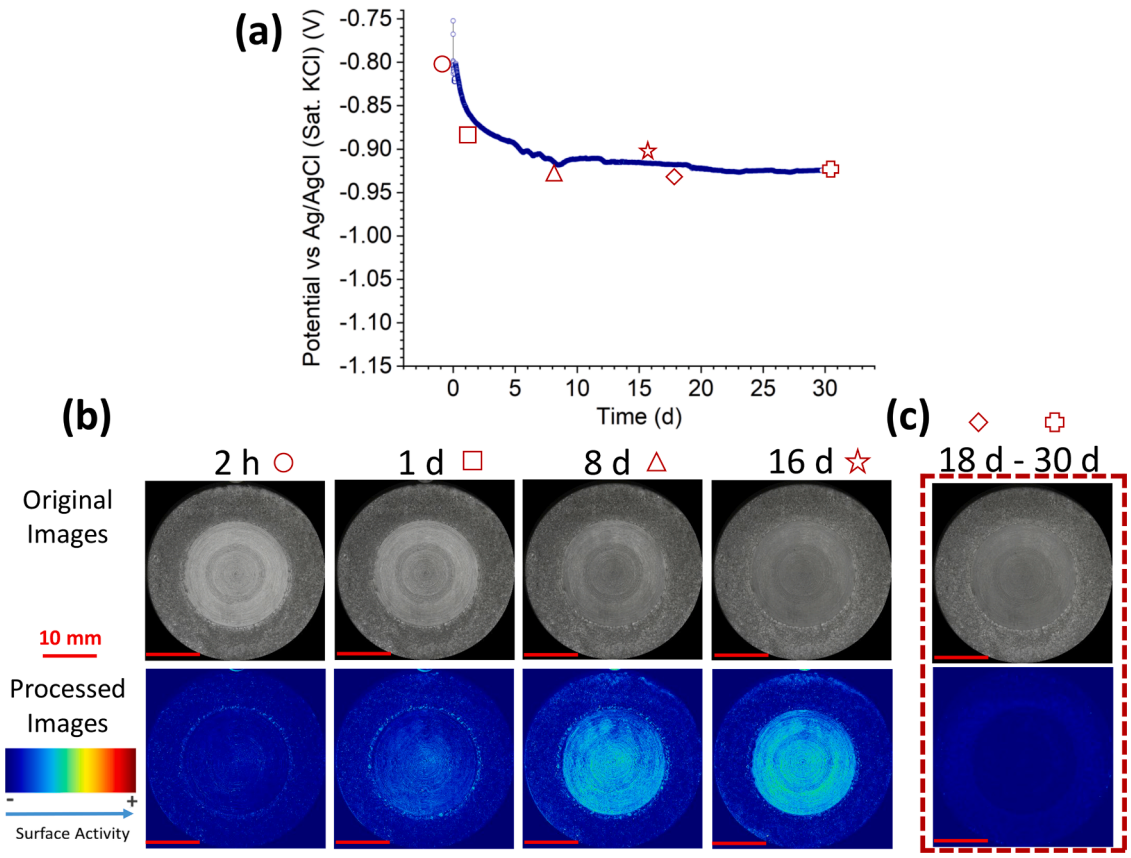

Fig. 8. Optical-Electrochemical monitoring of TSA with 30% of exposed steel after removing the calcareous deposits formed on the top of steel (C-30R). **(a)** Record of OCP. **(b)** Original and processed sequential images. **(c)** Optical analysis from 18 d to 30 d.

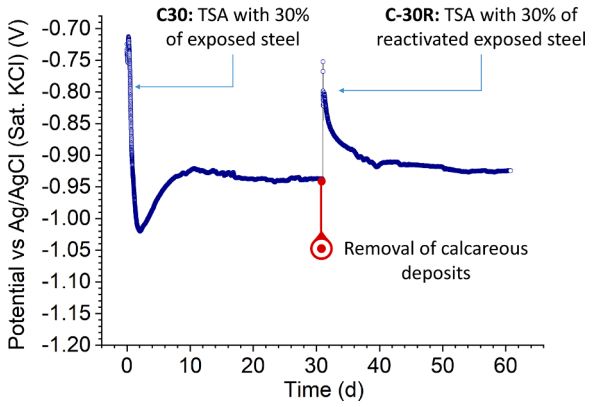

Fig. 9. OCP evolution of the damaged TSA and after removing the calcareous deposits. Samples C30 and C-30R, respectively.

- Iron dissolution takes place within the first few hours of exposure when the defect in TSA coating is machined before immersion. This process continues until the air-formed oxide layer deteriorates, causing the aluminum surface to become activated and the system to attain the recommended protection potential for steel. The time it takes for TSA to provide effective cathodic protection once the sample comes into contact with synthetic seawater increases when the defect size is larger.
- When the defect is created after exposure, the pores are clogged with aluminium corrosion products and/or calcareous deposits, reducing the self-corrosion of aluminium. However, rapid activation of TSA was observed providing immediate protection to the exposed steel even in presence of large defects.
- In all specimens with defects, the evolution of the potentials towards less negative values is directly associated with the formation of a layer of calcareous deposits on the exposed steel. The time of formation differed in each case, with smaller defects (5% exposed steel) exhibiting a shorter formation time than larger defects (30% exposed

Table 4
Time of formation of calcareous deposits in the exposed steel (optically recognizable) and recorded potential in each case.

Case	Fine layer of calcareous deposits		Dense layer of calcareous deposits		Plateu		Bubbling	
	Time (d)	Potential (V)	Time (d)	Potential (V)	Time (d)	Potential (V)	Coated zone	Defect zone
A0	3	-1.138	15	-1.034	18 to 35	-0.997	High	–
A-10	2	-0.969	7	-0.980	8 to 30	-0.965	Low	Low
B5[a]	1	-1.011	2	-1.060	13 to 35	-0.971	High	High
C30[b]	4	-0.986	14	-0.925	10 to 35	-0.938	High	Moderate
C-30R	1	-0.850	16	-0.916	8 to 30	-0.924	None	None

[a] Signs of iron oxidation at the beginning of the test. Protective potential (-0.743 V) reached after 2 h.
[b] Signs of iron oxidation at the beginning of the test. Protective potential (-0.743 V) reached after 7 h.

steel) that were machined before immersion. The presence of defects prior to immersion affected the cathodic reactions, leading to a faster formation of corrosion products and calcareous deposits than those defects created after exposure.
- Gravity plays a key role in the location of calcareous deposits when large defects are evaluated. These sparingly soluble deposits tend to sink to the bottom of the tank under the influence of gravity after being dislodged from the defect area. No corrosion or rust was seen in the defect area, providing evidence of the high damage tolerance of TSA.

CRediT Authorship Contribution Statement

Adriana Castro-Vargas: Conceptualization, Visualization, Methodology, Analysis, Writing, Original draft preparation. **Shiladitya Paul:** Conceptualization, Supervision, Review and Editing.

Declaration of Competing Interest

The authors declare that they have no known competing financial interests or personal relationships that could have appeared to influence the work reported in this paper.

Data availability

I have shared the link to my data.

Acknowledgements

This publication was made possible by the sponsorship and support of Lloyd's Register Foundation. Lloyd's Register Foundation helps to protect life and property by supporting engineering-related education, public engagement, and the application of research. The work was enabled through, and undertaken at, the National Structural Integrity Research Centre (NSIRC), a postgraduate engineering facility for industry-led research into structural integrity established and managed by TWI through a network of both national and international universities. The authors gratefully acknowledge the Colombian Ministry of Science, Technology, and Innovation (MinCiencias) for the financial support of Adriana Castro Vargas (Program No. 860-2019).

Supplementary materials

Supplementary material associated with this article can be found, in the online version, at doi:10.1016/j.electacta.2023.142847.

References

[1] W.H. Thomason, Offshore Corrosion Protection With Thermal-Sprayed Aluminum, Offshore Technology Conference Houston, Texas, 1985, doi:10.4043/4971-MS.
[2] D.K.K. Tiong, H. Pit, Experiences on Thermal Spray Aluminum (TSA) Coating on Offshore Structures, CORROSION (2004) 2004. OnePetro.
[3] K.P. Fischer, W.H. Thomason, T. Rosbrook, J. Murali, Performance history of thermal-sprayed aluminum coatings in offshore service, Materials performance 34 (1995) 27–35.
[4] D.N. Veritas, DNV-RP-B401 Cathodic Protection Design, Recommended Practice, Det Norske Veritas, Norway, 2005.
[5] A. Castro-Vargas, S. Gill, S. Paul, Effect of Corrosion Products and Deposits on the Damage Tolerance of TSA-Coated Steel in Artificial Seawater, Surfaces 5 (2022) 113–126, https://doi.org/10.3390/surfaces5010005.
[6] R. Grinon-Echaniz, P. Refait, M. Jeannin, R. Sabot, S. Paul, R. Thornton, Study of cathodic reactions in defects of thermal spray aluminium coatings on steel in artificial seawater, Corrosion Science 187 (2021), 109514, https://doi.org/10.1016/j.corsci.2021.109514.
[7] R. Grinon-Echaniz, S. Paul, R. Thornton, P. Refait, M. Jeannin, A. Rodriguez, Prediction of thermal spray coatings performance in marine environments by combination of laboratory and field tests, Coatings 11 (2021) 320, https://doi.org/10.3390/coatings11030320.
[8] R.G. Echaniz, S. Paul, R. Thornton, Effect of seawater constituents on the performance of thermal spray aluminum in marine environments, Materials and Corrosion 70 (2019) 996–1004, https://doi.org/10.1002/maco.201810764.
[9] S. Paul, Cathodic protection of offshore structures by extreme damage tolerant sacrificial coatings, CORROSION (2018) 2018. OnePetro.
[10] S. Paul, Behavior of damaged thermally sprayed aluminum (TSA) in aerated and deaerated seawater, CORROSION (2019) 2019. OnePetro.
[11] B. Syrek-Gerstenkorn, S. Paul, A.J. Davenport, Sacrificial thermally sprayed aluminium coatings for marine environments: A review, Coatings 10 (2020) 267, https://doi.org/10.3390/coatings10030267.
[12] Y. Yang, J.D. Scantlebury, E.V. Koroleva, A study of calcareous deposits on cathodically protected mild steel in artificial seawater, Metals 5 (2015) 439–456, https://doi.org/10.3390/met5010439.
[13] J.F. Yan, R.E. White, R. Griffin, Parametric studies of the formation of calcareous deposits on cathodically protected steel in seawater, Journal of the Electrochemical Society 140 (1993) 1275.
[14] W.R. Smith, S. Paul, Natural deposit coatings on steel during cathodic protection and hydrogen ingress, Coatings 5 (2015) 816–829, https://doi.org/10.3390/coatings5040816.
[15] C. Barchiche, C. Deslouis, D. Festy, O. Gil, P. Refait, S. Touzain, B. Tribollet, Characterization of calcareous deposits in artificial seawater by impedance techniques: 3—Deposit of CaCO3 in the presence of Mg (II), Electrochimica Acta 48 (2003) 1645–1654, https://doi.org/10.1016/S0013-4686(03)00075-6.
[16] N. Ce, S. Paul, The effect of temperature and local pH on calcareous deposit formation in damaged thermal spray aluminum (TSA) coatings and its implication on corrosion mitigation of offshore steel structures, Coatings 7 (2017) 52, https://doi.org/10.3390/coatings7040052.
[17] B. Syrek-Gerstenkorn, S. Paul, A.J. Davenport, Use of thermally sprayed aluminium (TSA) coatings to protect offshore structures in submerged and splash zones, Surface and Coatings Technology 374 (2019) 124–133, https://doi.org/10.1016/j.surfcoat.2019.04.048.
[18] H.S. Lee, J.K. Singh, J.H. Park, Pore blocking characteristics of corrosion products formed on Aluminum coating produced by arc thermal metal spray process in 3.5 wt.% NaCl solution, Construction and Building Materials, 113 (2016) 905-916, doi:10.1016/j.conbuildmat.2016.03.135.
[19] S. Paul, Hydrogen in aluminium-coated steels exposed to synthetic seawater, Surfaces 3 (2020) 282–300, https://doi.org/10.3390/surfaces3030021.
[20] S. Pedersen, J. Liniger, F.F. Sørensen, M. von Benzon, On Marine Growth Removal on Offshore Structures, OCEANS 2022-Chennai, IEEE, 2022, pp. 1–6.
[21] E. Abedi Esfahani, H. Salimijazi, M.A. Golozar, J. Mostaghimi, L. Pershin, Study of corrosion behavior of arc sprayed aluminum coating on mild steel, Journal of thermal spray technology 21 (2012) 1195–1202, https://doi.org/10.1007/s11666-012-9810-x.
[22] A. Gericke, M. Hauer, B. Ripsch, M. Irmer, J. Nehlsen, K.M. Henkel, Fatigue Strength of Structural Steel-Welded Connections with Arc-Sprayed Aluminum Coatings and Corrosion Behavior of the Corresponding Coatings in Sea Water, Journal of Marine Science and Engineering 10 (2022) 1731, https://doi.org/10.3390/jmse10111731.
[23] A. López-Ortega, R. Bayón, J. Arana, Evaluation of protective coatings for offshore applications. Corrosion and tribocorrosion behavior in synthetic seawater, Surface and Coatings Technology 349 (2018) 1083–1097, https://doi.org/10.1016/j.surfcoat.2018.06.089.
[24] S. Paul, D. Harvey, Determination of the Corrosion Rate of Thermally Spayed Aluminum (TSA) in Simulated Marine Service, CORROSION (2020) 2020. OnePetro.
[25] ISO, 8501-1, Preparation of steel substrates before application of paints and related products—Visual assessment of surface cleanliness—Part 1: Rust grades and preparation grades of uncoated steel substrates and of steel substrates after overall removal of previous coatings, 2007.
[26] ASTM D1141-98, Standard practice for the preparation of substitute ocean water, ASTM International, 2013.
[27] D. Tejero-Martin, M. Rezvani Rad, A. McDonald, T. Hussain, Beyond traditional coatings: a review on thermal-sprayed functional and smart coatings, Journal of Thermal Spray Technology 28 (2019) 598–644.
[28] M. Smith, Comparing cold spray with thermal spray coating technologies, The cold spray materials deposition process, Elsevier, 2007, pp. 43–46, https://doi.org/10.1533/9781845693787.1.43.